THE UNIVERSITY OF AUCKLAND
FACULTY OF SCIENCE

UpWind

Work Package 6.2 under the European Commission Integrated Wind Turbine Design (UPWIND)

Traceable Calibration for Monostatic SODAR and LIDAR: In situ Calibration of SODARs via Level Perturbation

Stuart Bradley

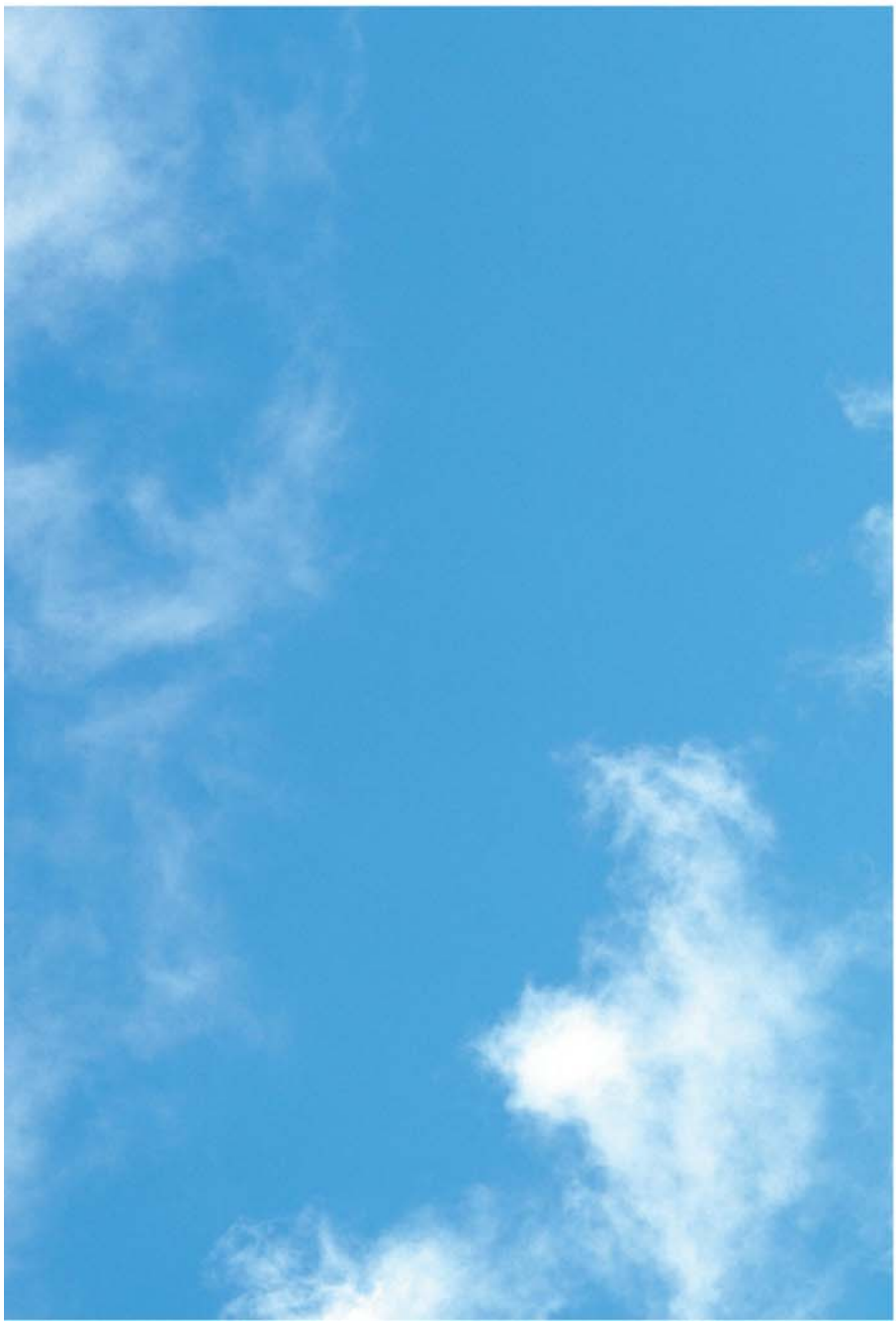

Contents

1. Introduction

Commercially available SODARs transmit a short pulse in at least three upward directions. Scattering from atmospheric turbulent refractive index fluctuations results in a time series signal from each direction. Spectral analysis of time-gated segments of these time series gives a spectral peak which is a measure of the turbulent strength and whose frequency is a measure of the Doppler shift experienced by the moving scatterers. Using at least three independent acoustic beams assures a system of at least three equations in the vector wind Cartesian components $\boldsymbol{V} = (u, v, w)$. Solving this set of equations then gives a wind profile with estimates at the centre of each height represented by the centre of each time gate [1].

There is very little that can 'go wrong' with such a simple remote-sensing arrangement since the only real decision required is the position of each spectral peak. Peak position estimation in the presence of some background noise is a well-established procedure. Nevertheless, large efforts have been expended on comparisons between mast-mounted anemometers and SODARs in such experiments as PIE [2]. There are a number of reasons for this work, including the desire to ultimately have remote-sensing recognized as a viable replacement for well-established mast instrumentation, and the problems with variable treatment of background noise problems. The latter include random acoustic noise and unwanted reflections from rain or fixed objects near to the SODAR. Unwanted reflections can, however, be largely removed by judicious use of software filters, leaving mostly the random noise component. Some of this random component is actually due to atmospheric fluctuations (i.e the assumption that there should be a very narrow spread in wind velocity over an averaging period may be false).

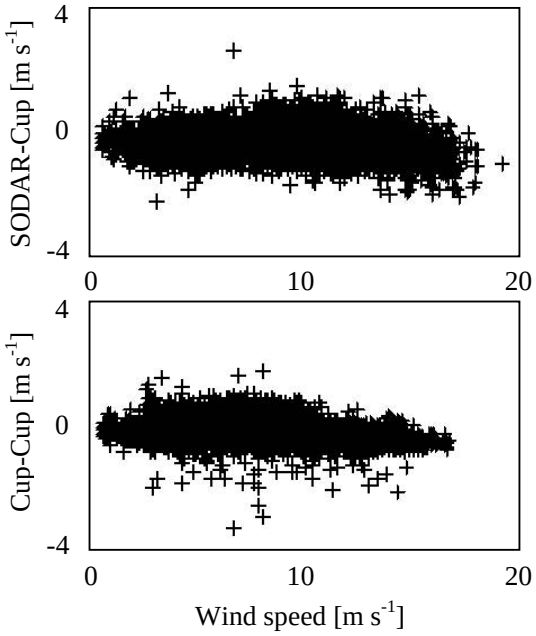

Figure 1a. Residual plots for a SODAR compared with a mast-mounted cup anemometer (upper plot) and for two cup anemometers (lower plot) at 60m.

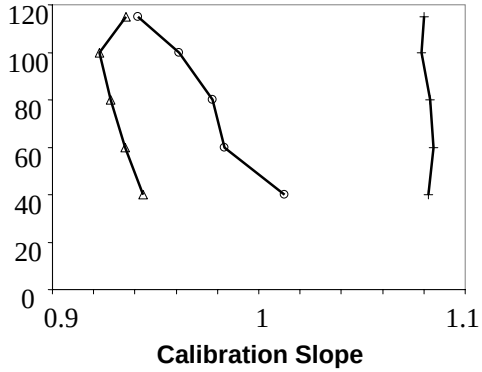

Figure 1b. Variation in calibration slope with height for three different SODAR models.

The most important findings of the WISE/PIE work were that a SODAR gives similar variability in wind speeds to a cup anemometer (Fig. 1a), and there remain (small) *systematic* errors in wind speeds estimated by a SODAR (Fig 1b).

The major challenge for SODAR calibration is therefore to remove these systematic biases. Such biases can obviously be detected through SODAR-mast comparisons, but these are in general rather inconvenient. Therefore, in this paper, we consider a new method for doing *in-situ* field calibrations of a SODAR. This method has the huge advantage of not requiring comparison against some other 'standard', nor requiring any assumptions regarding SODAR geometry and operation.

2. SODAR calibration

2.1 Traditional calibration against mast-mounted instruments

Monostatic SODARs (and LIDARs) use beams tilted from the vertical. The signal scattered back to the receiver in each tilted beam is Doppler-shifted according to the component V_r of wind velocity $\boldsymbol{V}$ in the beam direction. For a thin beam in direction $\boldsymbol{\Omega_0} = (\cos\phi_0 \sin\theta_0, \sin\phi_0 \sin\theta_0, \cos\theta_0)$ and wind velocity $\boldsymbol{V} = (u, v, w)$

$$V_r = \boldsymbol{V} \bullet \boldsymbol{\Omega_0} = u\cos\phi_0 \sin\theta_0 + v\sin\phi_0 \sin\theta_0 + w\cos\theta_0 \tag{1}$$

At least 3 independent measurements are needed to solve for *u*, *v*, and *w*, and, for the purposes of this paper, we will concentrate on the typical 3-beam design. The system of equations

$$\boldsymbol{R} = \boldsymbol{B}\boldsymbol{V} \tag{2}$$

is solved, where $\boldsymbol{R}$ is the 3x1 vector of measured radial velocity components, $\boldsymbol{B}$ is the 3x3 weighting matrix, and $\boldsymbol{V}$ is the 3x1 vector of unknown wind velocity components *u*, *v*, and *w*. The solution $\hat{\boldsymbol{V}} = \boldsymbol{B}^{-1}\boldsymbol{R}$ is used to form $\left(\hat{u}^2 + \hat{v}^2 + \hat{w}^2\right)^{1/2} = \left(\hat{\boldsymbol{V}} \bullet \hat{\boldsymbol{V}}\right)^{1/2}$ for comparison with $\left(u^2 + v^2 + w^2\right)^{1/2} = \left(\boldsymbol{V} \bullet \boldsymbol{V}\right)^{1/2}$ measured by a mast-mounted cup anemometer. By this method a *single* calibration slope

$$m = \left(\hat{\boldsymbol{V}} \bullet \hat{\boldsymbol{V}}\right)^{1/2} / \left(\boldsymbol{V} \bullet \boldsymbol{V}\right)^{1/2} \tag{3}$$

is obtained.

Consider the following simple example. A very narrow beam in the *x*-*z* plane, and with $w = 0$ has $V_r = u \sin\theta_0$ so the wind estimate is $\hat{u} = V_r / \sin\theta_0$. If there is an uncertainty or an error $\Delta\theta$ in the tilt angle θ_0, then the uncertainty or error in estimated wind is $\Delta\hat{u}/\hat{u} = -\Delta\theta / \tan\theta_0$. For θ_0 =15°, each 1° error in beam pointing angle gives a 5% error in estimation of wind speed: Monostatic SODARs and LIDARs are ***highly sensitive*** to beam pointing.

2.2 Complete calibration

The single calibration slope *m* in (3) contains combinations of the 9 elements from beam matrix ***B***. In obtaining estimates of *u*, *v*, and *w*, these elements are *assumed* known in the SODAR processing software. A misunderstanding of the value of any one of these 9 elements could give a variation in *m*. This variation in *m* will also be *wind-direction dependent* as can be seen from the very simple case of a beam tilted an angle θ_0 in the *x-z* plane, another beam tilted θ_0 in the *y-z* plane, and the third beam vertical. Then

$$m^2 = \left(\frac{\hat{V}}{V}\right)^2 = \frac{\sin^2\theta_0}{\sin^2\hat{\theta}} + \frac{w\left(\cos\theta_0 - \cos\hat{\theta}\right)\left[2(u+v)\sin\theta_0 + w\left(2+\cos\theta_0+\cos\hat{\theta}\right)\right]}{\left(u^2+v^2+w^2\right)\sin^2\hat{\theta}} \quad (4)$$

where $\hat{\theta}$ is the tilt angle assumed by the software, and θ_0 is the actual tilt angle. This problem with traditional calibration methods has not been previously considered.

In practice however, the beam is not an angular delta-function and the weights in (1) are volume averages over the transmitted and received beams

$$V_r = u\overline{\cos\phi\sin\theta} + v\overline{\sin\phi\sin\theta} + w\overline{\cos\theta}\,. \quad (5)$$

The resulting matrix of 9 volume-averaged weights forms ***a complete set*** of calibration constants for wind profiling.

There is an obvious need to provide a method by which more detailed calibration information, involving the full matrix *B*, is obtained. This could be done in principle by measuring the beam angular intensity variations in an anechoic chamber, or perhaps in the field, but this effort would be large because of the need to capture beam details on a hemispherical surface in high angular resolution in 2D so that the proper volume averages can be calculated.

3. Tilt angle perturbation

3.1 Basic perturbation concept

Figure 2 shows the *x-z* plane for a SODAR having a beam at an initial effective tilt angle θ_1. If there is also a beam in the *y-z* plane tilted at an angle of θ_2 to the vertical, the equations corresponding to (1) are

$$V_{r1} = u\sin\theta_1 + w\cos\theta_1 \quad (6)$$

$$V_{r2} = v\sin\theta_2 + w\cos\theta_2 \quad (7)$$

$$V_{r3} = w \quad (8)$$

Also shown is the entire SODAR rotated by an angle $\Delta\theta$ about the *y* axis. Now (6)-(8) become

$$V^*_{r1} = u\sin(\theta_1+\Delta\theta) + w\cos(\theta_1+\Delta\theta) \quad (9)$$

$$V^*_{r2} = u\sin(\Delta\theta)\cos\theta_2 + v\sin\theta_2 + w\cos(\Delta\theta)\cos\theta_2 \quad (10)$$

$$V^*_{r3} = u\sin(\Delta\theta) + w\cos(\Delta\theta) \quad (11)$$

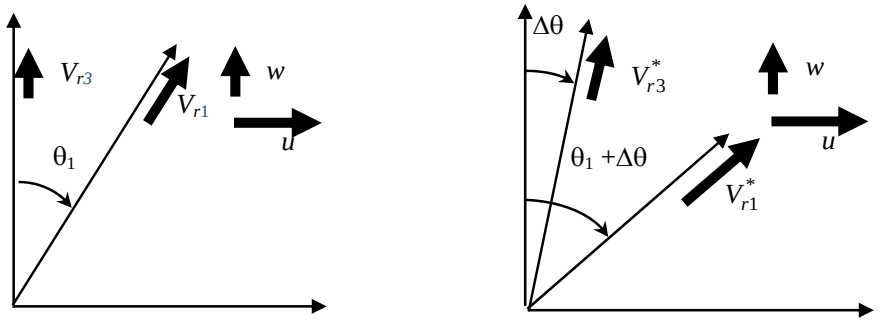

Figure 2. *The geometry of a SODAR beam tilted at an angle θ_1 (left diagram) and with the SODAR rotated by an angle $\Delta\theta$ about the y axis (right diagram). The wind velocity components in this plane are u and w, and the along-beam radial components for the two beams in this plane are V_{r1} and V_{r3}.*

The $V_{r1}, V_{r3}, V^*_{r1}, V^*_{r3}$ quantities are measured, the tilt angle perturbation $\Delta\theta$ is known, and the quantities u, w, θ_1 and θ_2 are unknown. Equations (6) through (11) are non-linear in the unknowns, but can be solved by finding: w from (8); u from (11); $\sin\theta_1$ from (6) and (9); $\cos\theta_2$ from (7) and (10); and v from(7). This gives

$$u = \frac{V^*_{r3} - V_{r3}\cos\Delta\theta}{\sin\Delta\theta}. \tag{12}$$

$$v = \frac{\left(V_{r2}V^*_{r3} - V_{r3}V^*_{r2}\right)\left(V^*_{r3} - V_{r3}\right)}{\sqrt{\left(V^*_{r3} - V_{r3}\right)^2 - \left(V^*_{r2} - V_{r2}\right)^2}} \tag{13}$$

$$w = V_{r3} \tag{14}$$

$$\sin\theta_1 = \frac{V_{r1}V^*_{r3} - V^*_{r1}V_{r3}}{V^2_{r3} - 2V_{r3}V^*_{r3}\cos\Delta\theta + V^{*2}_{r3}}\sin\Delta\theta \tag{15}$$

$$\cos\theta_2 = \frac{V^*_{r2} - V_{r2}}{V^*_{r3} - V_{r3}} \tag{16}$$

3.2 The effective tilt angle

As indicted above in (5), the components of beam matrix $\boldsymbol{B}$ are volume averages. In (6) – (16) this volume averaging appears to have been ignored. The volume averaging means that a normalized beam gain function $G(\boldsymbol{\Omega}, \boldsymbol{\Omega_0})$ is averaged over solid angle $\boldsymbol{\Omega}$ around a pointing direction $\boldsymbol{\Omega_0}$ in each of the terms on the right of (1):

$$\begin{aligned} V_r &= \int_\Omega \boldsymbol{b}\bullet\boldsymbol{V}G(\boldsymbol{\Omega},\boldsymbol{\Omega_0})d\Omega \\ &= \int_\Omega \left(u\cos\phi\sin\theta + v\sin\phi\sin\theta + w\cos\theta\right)G(\boldsymbol{\Omega},\boldsymbol{\Omega_0})d\Omega \\ &= u\int_\Omega \cos\phi\sin\theta G(\boldsymbol{\Omega},\boldsymbol{\Omega_0})d\Omega + v\int_\Omega \sin\phi\sin\theta G(\boldsymbol{\Omega},\boldsymbol{\Omega_0})d\Omega + w\int_\Omega \cos\theta G(\boldsymbol{\Omega},\boldsymbol{\Omega_0})d\Omega \\ &= u\overline{\cos\phi\sin\theta} + v\overline{\sin\phi\sin\theta} + w\overline{\cos\theta} \end{aligned} \tag{17}$$

where

$$\int_{\Omega} G(\mathbf{\Omega}, \mathbf{\Omega_0}) d\Omega = 1 \tag{18}$$

For a beam nominally in the *x*-*z* plane, there will be contributions from finite azimuth angles ϕ. However, such beams are invariably symmetric in azimuth, so *G* is an even function of ϕ and the integral

$$\int_{\Omega} \sin\phi \sin\theta G(\mathbf{\Omega}, \mathbf{\Omega_0}) d\Omega = 0 \tag{19}$$

This means that, for this beam,

$$V_r = u\overline{\cos\phi \sin\theta} + w\overline{\cos\theta} = u\sin\theta_1 + w\cos\theta_1 \tag{20}$$

The θ_1 appearing in (6) is therefore an *effective* beam tilt angle. If this is perturbed by rotating the entire SODAR through $\Delta\theta$ about the *y* axis then, using an angular coordinate system attached to the SODAR, $G(\mathbf{\Omega}, \mathbf{\Omega_0})$ remains unchanged but the beam direction with respect to the wind $\boldsymbol{V}$ is now $(\cos\phi\sin[\theta+\Delta\theta], \sin\phi\sin[\theta+\Delta\theta], \cos[\theta+\Delta\theta])$. The first term on the right of (17) becomes

$$\begin{aligned}
&u\int_{\Omega} \cos\phi \sin(\theta+\Delta\theta) G(\mathbf{\Omega}, \mathbf{\Omega_0}) d\Omega \\
&\quad = u\int_{\Omega} \cos\phi (\sin\theta\cos\Delta\theta + \cos\theta\sin\Delta\theta) G(\mathbf{\Omega}, \mathbf{\Omega_0}) d\Omega \\
&\quad = u\cos\Delta\theta \int_{\Omega} \cos\phi\sin\theta G(\mathbf{\Omega}, \mathbf{\Omega_0}) d\Omega + u\sin\Delta\theta \int_{\Omega} \cos\phi\cos\theta G(\mathbf{\Omega}, \mathbf{\Omega_0}) d\Omega \\
&\quad = u\cos\Delta\theta \overline{\cos\phi\sin\theta} + u\sin\Delta\theta \overline{\cos\phi\cos\theta} \\
&\quad = u\cos\Delta\theta\sin\theta_1 + u\sin\Delta\theta\cos\theta_1 \\
&\quad = u\sin(\theta_1 + \Delta\theta)
\end{aligned} \tag{21}$$

This means that, although θ_1 is an effective zenith angle and not necessarily the same as the pointing zenith angle, we can validly do arithmetic such as $\sin(\theta_1+\Delta\theta) = \sin\theta_1\cos\Delta\theta + \cos\theta_1\sin\Delta\theta$ as in (6)-(16) above.

4. The effect of beam geometry on Doppler shift

In the above, the Doppler shift is contained in the elements of vector ***R***. The weighting on each of the wind velocity components is volume-averaged, but this does not give any indication of the spread or shape of the Doppler spectrum from which, by detecting the peak position, the components of ***R*** are estimated. The acoustic radar equation covers this in principle [1], but we will first briefly go through the basics because the frequency-dependence is not usually evident.

The acoustic power transmitted has a frequency-dependent spectral density which can be approximated by

$$\frac{dP_T}{df} = E\exp\left[-\frac{1}{2\sigma_f^2}(f - f_T)^2\right] \tag{22}$$

where E is the spectral amplitude, f is frequency, σ_f is the spectral width, and f_T the frequency of the transmitted pulse. The power per unit frequency interval transmitted into solid angle $d\Omega$ is

$$\frac{dP_T}{df} G_a d\Omega ,$$

for an antenna gain G_a, the sound intensity at range r is

$$\frac{dP_T}{df} G_a \frac{e^{-\alpha r}}{r^2}$$

(where α is the acoustic absorption), the power scattered into solid angle $\Delta\Omega_s$ is

$$\frac{dP_T}{df} G_a \frac{e^{-\alpha r}}{r^2} \sigma_s \Delta\Omega_s \Delta V$$

(where σ_s is the scattering cross-section area per unit volume and per unit solid angle, and ΔV is the scattering volume), and the spectral density of received power at the same (mono-static) antenna

$$\frac{dP_R}{df} = \int_\Omega \frac{dP_T}{df} G_a \frac{e^{-\alpha r}}{r^2} \sigma_s \left(\frac{A_e}{r^2} \right) \left(r^2 d\Omega c\tau \right) e^{-\alpha r} \tag{23}$$

(where A_e is the effective receiving antenna area, allowing for efficiency and orientation, c is the speed of sound, and τ is the pulse duration). Allowing for Doppler shifting of the spectrum to be centered on f_D rather than f_T,

$$\frac{dP_R}{df} = Ec\tau \frac{e^{-2\alpha r}}{r^2} \sigma_s \int_\Omega \exp\left[-\frac{1}{2\sigma_f^2} (f - f_D)^2 \right] G(\boldsymbol{\Omega}) d\Omega \tag{24}$$

where $G = G_a A_e / A$ is an angle-dependent sensitivity kernel and the actual receiving antenna area is A. The atmospheric absorption and scattering parts have been taken outside of the scattering volume integral since they are only weakly frequency-dependent and it is assumed that they do not vary much within a typical scattering volume. However, the Doppler-shifted echo frequency f_D, and the antenna angular sensitivity G will vary with beam pointing direction.

For example, if the acoustic beam has sensitivity G at a zenith angle θ and azimuth angle ϕ, then the integral is

$$\int_0^{2\pi} \left\{ \int_{-\frac{\pi}{2}}^{\frac{\pi}{2}} \exp\left[-\frac{1}{2\sigma_f^2} \left[f - f_T \left(1 - 2\frac{u}{c} \sin\theta\cos\phi - 2\frac{v}{c} \sin\theta\sin\phi - 2\frac{w}{c} \cos\theta \right) \right]^2 \right] G \sin\theta d\theta \right\} d\phi \tag{25}$$

The usual assumption is that the beam in the x-z plane is effectively an angular delta-function

$$G(\theta, \phi) = \cos\theta \delta(\theta - \theta_0) \delta(\phi) \tag{26}$$

Then the above integral becomes

$$\exp\left[-\frac{1}{2\sigma_f^2} \left[f - f_T \left(1 - 2\frac{u}{c} \sin\theta_0 - 2\frac{w}{c} \cos\theta_0 \right) \right]^2 \right] \sin\theta_0 \cos\theta_0$$

so that the spectrum peaks at

$$f_x = f_T \left(1 - 2\frac{u}{c} \sin\theta_0 - 2\frac{w}{c} \cos\theta_0 \right) \tag{27}$$

giving the expected radial component as in (1) with $\phi_0 = 0$. Similarly, it is usually assumed that the beam in the $+z$ direction has the form $G(\theta, \phi) = \delta(\theta)\delta(\phi)$ so that that spectrum peaks at

$$f_z = f_T\left(1-2\frac{w}{c}\right). \tag{28}$$

More generally, it can be seen in (25) that there is a term in $\sin^2\phi$ so that there is a contribution from the traverse width of the beam in spite of G being even in ϕ. The influence of this term in v is to give a broader spectral peak but not to change the peak position, so will be ignored in the following. Also, in general the effect of the $\sin\theta$ weighting on u is to bias the spectral peak to the equivalent of a larger effective θ_0.. There is therefore a small change in the effective tilt angle, as expected. However, this does not change the methodology of the new calibration concept when the effective tilt angle is unknown anyway.

5. Error analysis

Writing σ_V for the uncertainty in wind speed V, (15) gives

$$\sigma_{\theta_1}^2 \approx \left(\frac{\tan\theta_1}{\tan\Delta\theta}\right)^2\left[\sigma_{\Delta\theta}^2+\left(\frac{\sigma_V\sin\theta_1}{V}\right)^2\right] \tag{29}$$

In order to achieve a calibration accuracy of 1%, we need $\sigma_\theta \approx 0.2° \approx 4\text{x}10^{-3}$ radian. For $\theta_1 = \Delta\theta = 15°$, and without any peak detection error, $\Delta\theta$ also needs to be measured to 0.2°. This is achievable with a linear actuator and a digital inclinometer. The accuracy of the SODAR spectral peak estimation for 10-minute averages is typically $\sigma_V = 0.2$ m s^{-1}, so the term in σ_V is typically a factor of 10 larger than the $\sigma_{\Delta\theta}$ term. What this means is that around 10 trials of 10-minute duration must be conducted in order to reduce the typical errors from peak detection to an acceptable level.

An alternative is to recast (15) in the form

$$y = ax \tag{30}$$

where

$$y = \frac{V_{r3}^2 - 2V_{r3}V_{r3}^*\cos\Delta\theta + V_{r3}^{*2}}{V_{r1}V_{r3}^* - V_{r1}^*V_{r3}} \tag{31}$$

and $x = \sin\Delta\theta$. Then the slope of the least-squares line through the origin is $a = 1/\sin\theta_1$.

A disadvantage of this method is that the radial velocity components may not be made available to the user by the SODAR manufacturer. This means that they need to be calculated based on the beam zenith angle assumed by the manufacturer (which is usually given), or the zenith angle calculated from the antenna parameters. This use of the expected zenith angle means that the method is not quite 'blind' since it requires an assumption. An alternative, and much simpler procedure, is to assume that, in comparison with u and v, w is negligible, so

$$\frac{u^*}{u} - \cos\Delta\theta = \left(\frac{1}{\tan\theta_1}\right)\sin\Delta\theta \tag{32}$$

which means that θ_1 can be estimated from the slope of the straight-line fit through the origin, via

$$\tan\theta_1 = \frac{\sum_{n=1}^{N}(\sin\Delta\theta_n)^2}{\sum_{n=1}^{N}\left(\frac{u_n^*}{u_n} - \cos\Delta\theta_n\right)\sin\Delta\theta_n} \tag{33}$$

In this case

$$\sigma_{\theta_1}^2 \approx \frac{2}{\sum_{n=1}^{N} \sin^2 \Delta\theta_n} \left(\frac{\tan^2 \theta_1}{1+\tan^2 \theta_1} \right)^2 \left(\frac{\sigma_V}{V} \right)^2 \quad (34)$$

where N measurements are taken at $\Delta\theta_n$, n=1,2,…,N. For θ_1 = 15°, and σ_V/V = 0.04, three cycles of $\Delta\theta$ = 15° and 38° should give σ_θ < 0.2°.

6. Field measurements on a SODAR

Field measurements have been completed on an AeroVironment 4000 SODAR by mounting the SODAR on a frame, which is then tilted using a 12V-powered linear actuator, as shown in Figure 3. The operator used a reversing switch to raise and lower the tilting platform. Each time the actuator was stopped, the digital level value was recorded. The raising and lowering of the platform was synchronised with the SODAR averaging time, so that one undisturbed averaging period was followed by an averaging period in which the actuator was moved. A typical plot of tilt angle $\Delta\theta$ and of wind speed vs time is shown in Fig. 4.

Figure 3. *The mounting frame and linear actuator, with digital level (left photograph) and measurements being taken (right photograph).*

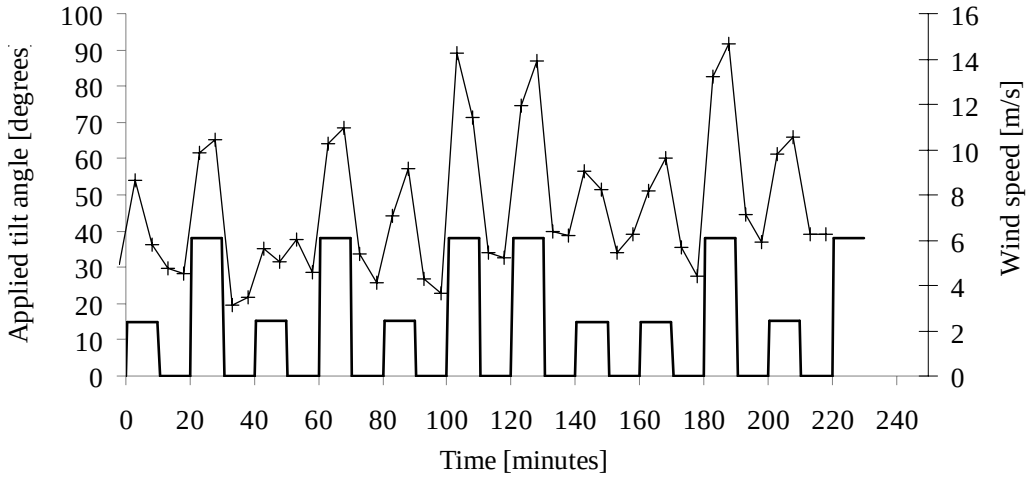

Figure 4. *Wind speed (crosses) and tilt angle (solid line) plotted as a function of time. Two distinct values of tilt angle were applied in this case.*

7. Data analysis

A sequence of 12 applied tilt angles were used as shown in Fig. 4 on an AeroVironment 4000 SODAR located at the Risø Hovesøre test site on very flat land in western Denmark. Wind vector components were recorded at 10 m height intervals from 30 m to 150 m. The top two heights generally contained some bad data and so were discarded. The processing described above was applied with the beam zenith angle θ_1 estimated from the least-squares slope of the line through the origin for both the $w = 0$ case and the full solution case. The variance of the y values corresponding to each of the two tilt angles was used as least-squares weights, since it was expected that the radial wind variability would increase as the SODAR was tilted further. Figure 5 shows the resulting estimated θ_1 values at each height for the two cases. As can be seen, the lowest height gives outlier values of angle: this is consistent with some clutter contamination from beam side-lobes when the beam is tilted. The estimated angle at the upper height (130 m) also appears to give an outlier, especially for the $w = 0$ case: this is consistent with the signal-to-noise ratio for SODAR signals decreasing rapidly above 120 m on the particular day recording were made (see Fig. 6).

The expected value of θ_1 can be calculated from the phased-array geometry for this SODAR. An incremental phase shift of $\pi/2$ is used to change beam zenith angles. The beam maximum will therefore be at a zenith angle of $\theta_1 = \sin^{-1}(\lambda/4d)$ where λ is the wavelength and d is the array element spacing. In the case of this SODAR, the transmitted frequency was 4500 Hz, and the speakers have a diameter of 0.085 m but are used in diagonal rows of spacing $d = 0.085/2^{1/2} =$ 0.06 m. Taking into account the mean air temperature at SODAR height during the experiment, $\theta_1 = 18.32°$. This compares with the estimated zenith angle from the two cases given in Table 1.

	Mean θ_1	$\sigma_{\text{mean }\theta}$	Estimated-calculated θ_1
Calculated θ_1	18.32°		
θ_1 estimated with $w = 0$	18.27°	0.23°	-0.05°
θ_1 estimated with $w \neq 0$	18.55°	0.54°	0.23°

Table 1. *Comparison between estimated beam zenith angles and the calculated zenith angle.*

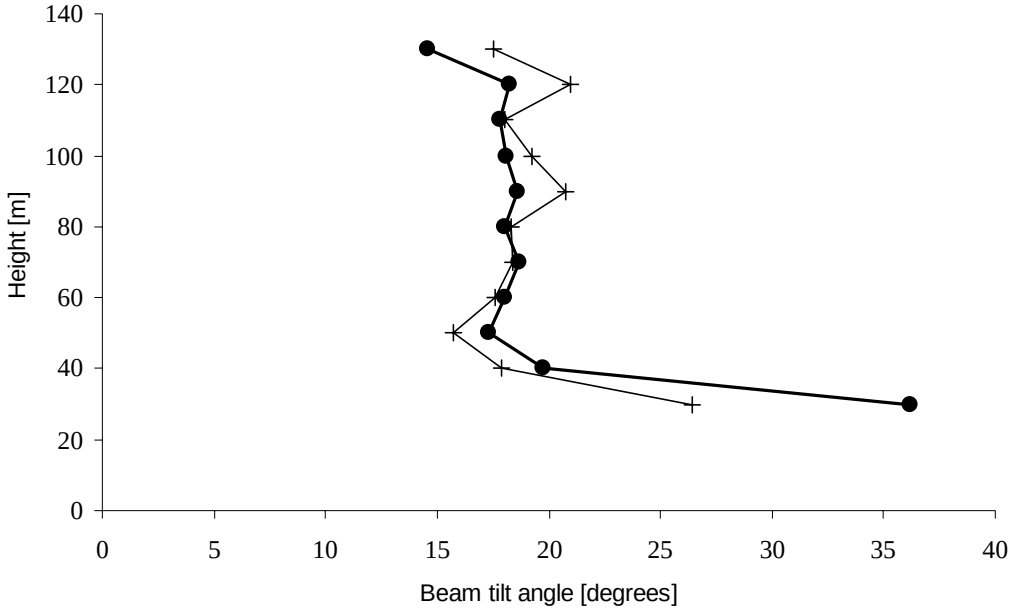

Figure 5. *Estimated beam zenith angles θ_1 from the w=0 case (filled circles) and the unconstrained w case (plus signs).*

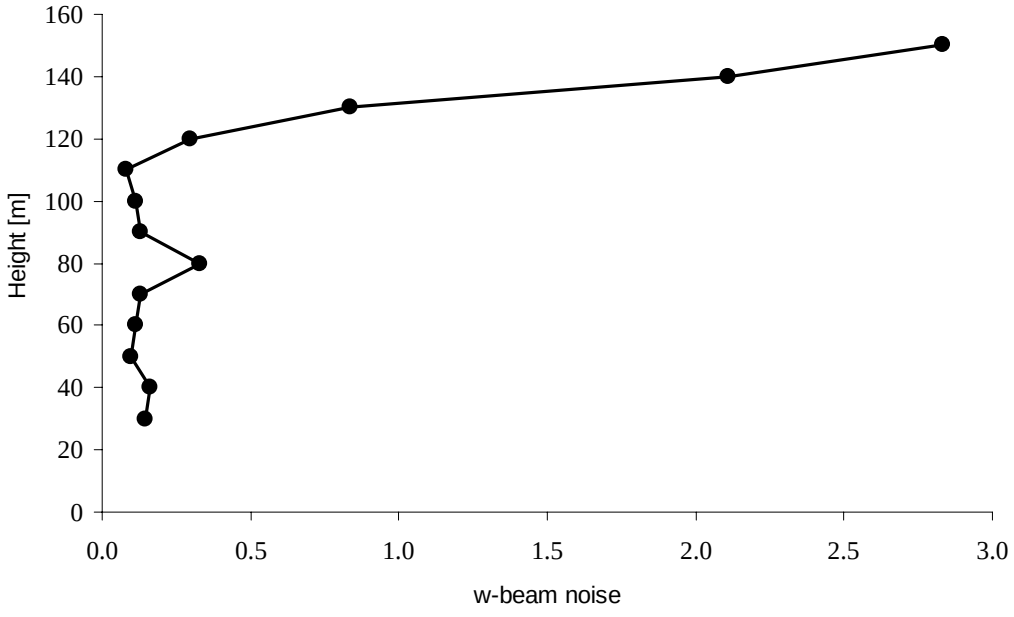

Figure 6. *The mean noise figure for the w beam as a function of height (bad data cases have been omitted).*

8. Conclusions

Since Doppler measurement is inherently calculable, the main source of systematic calibration errors for SODARs (and the reason so many mast comparisons have been performed) is uncertainty regarding the effective beam pointing angle.

A new method for *absolute* calibration of SODARs is described. The method makes no assumptions whatsoever about the SODAR operation and its hardware and software, other than the assumption that only one beam is transmitted at a time. Regardless of the complexity of the actual beam shape, the *effective* beam tilt angle is accurately estimated: this is the angle which must be used in estimations of velocity components. In a very simple experiment involving only 12 tilting events, the effective beam zenith angle has been found to within around 0.2°, which is as good as is required in the most stringent SODAR calibration procedures. It has been found, even for such a short data run, that the estimated angle, based on totally blind calibration, is very close to that calculated from the SODAR array geometry.

No additional electronics is required except to operate the linear actuator and record the angle using a digital inclinometer or, in our test example, a digital level. The linear actuator now being used is inexpensive and compact (can easily be carried in one hand). We are also currently designing a very simple mounting which can be used on any SODAR.

The only limitation evident at this stage is the requirement for horizontally stratified flow, since the regression methods use both a tilted beam and a vertical beam.

We are also considering the application for SODARs such as the AQS which do not have a vertical beam: this is a simple modification of the regression equations.

9. References

[1] Bradley S. G. *Atmospheric Acoustic Remote Sensing*. Florida, CRC Press/Taylor and Francis Group, 271pp., 2007. ISBN 978-0-8493-3588-4.

[2] Bradley S.G. (Ed), I. Antoniou, S. von Hünerbein, D. Kindler, M. de Noord, and H. E. Jørgensen, 2005: SODAR calibration for wind energy applications. Manchester, UK, *University of Salford*. 69pp.